Geometric Considerations of Micro- to Nanoscale Elastomeric Post Arrays to Study Cellular Traction Forces**

By *Michael T. Yang*, *Nathan J. Sniadecki*, and *Christopher S. Chen**

Mechanical interactions between cells and their surrounding extracellular matrix (ECM) play an important role in regulating many cellular functions, such as migration, proliferation and differentiation.[1–3] Cells adhere to a substrate through an integrated process that involves binding and clustering of integrins to ECM ligands,[4–5] actin polymerization-driven plasma membrane extension,[6–7] and contraction of the actomyosin cytoskeleton which transmits traction forces to the substrate through sites of adhesion.[8–9] Interestingly, mechanical properties of the substrate, such as stiffness and ECM ligand topology, feedback to affect the ability of cells to exert these forces and spread across the substrate.[10–11]

To elucidate the relationship between substrate mechanics, cell adhesion and traction forces, several approaches have been developed and continually refined. The first approach was to engineer soft materials such as partially crosslinked silicone elastomers and polyacrylamide gels.[9,12–13] Cells cultured on these substrates generated deformations that could be mapped by the displacement of embedded fluorescent markers and used to calculate traction forces.[9,14] In contrast to the continuous elastic substrata method, we pioneered another approach using microfabrication tools to develop an elastomeric micropost array (mPADs).[15] Cells cultured on this substrate deflect underlying posts as they contract. Traction forces could be calculated from these post deflections using a simple force-displacement relationship for pure bending of an elastic cylindrical beam (Eq. 1),

$$F = \left(\frac{3}{64}\pi E \frac{D^4}{L^3}\right)v \tag{1}$$

in which F, E, D, L, v are the bending force, Young's modulus, diameter, height and resulting deflection of the post. This relation further indicates that post stiffness could be tuned by altering the post geometry without changing material properties.

Despite their advantages, micropost-based substrates have drawbacks. The mPADs were micromolded from masters made up of arrays of SU-8 posts with a diameter of 3 μm and a center-to-center spacing of 9 μm.[15] The large post spacing constrained the shapes of adherent cells, affected their motility and limited the spatial resolution of the resultant traction force maps. To address these concerns, different microfabrication process flows have been developed to fabricate higher density arrays of smaller posts. By incorporating a contrast enhancement agent into SU-8 photolithography, arrays of SU-8 posts with a diameter of 2 μm and center-to-center spacing of 5–6 μm have been produced.[16] Achieving even higher density arrays with SU-8-based micromolding methods is difficult due to diffraction effects and other process factors in patterning tall SU-8 structures.[17] To overcome this limitation, conventional photolithography and deep reactive ion etching have been used to fabricate arrays of holes in silicon, from which posts with diameters as small as 1 μm and center-to-center distances of 3 μm have been cast.[18–19] By scaling down micropost array geometries, not only is stiffness affected, but parameters such as adhesive surface
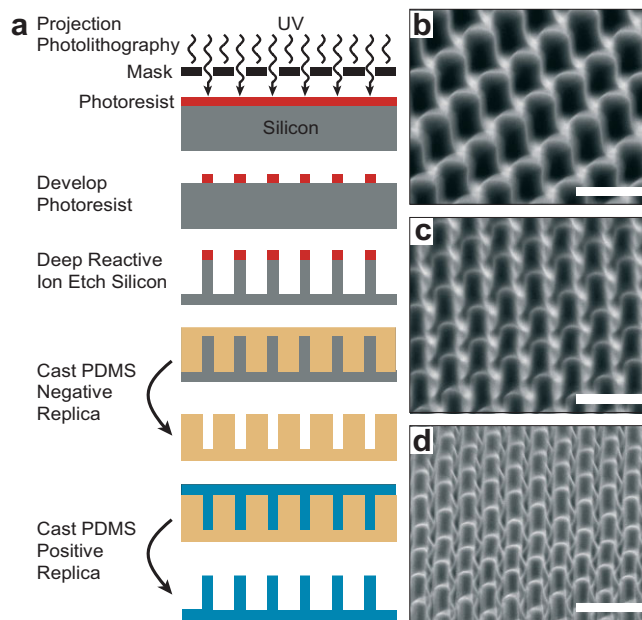

Figure 1. Fabrication of elastomeric nanopost arrays. a) Schematic of the microfabrication process used to generate PDMS nanopost arrays. Drawings are not to scale. b–d) SEM images of PDMS nanopost arrays with target post diameters of 1.5, 1 and 0.75 μm, and center-to-center spacings of 2.5, 2 and 1.5 μm, respectively. Scale bars are 3 μm.

[*] Prof. C. S. Chen, M. T. Yang, N. J. Sniadecki
Department of Bioengineering, University of Pennsylvania
210 S. 33rd Street, Philadelphia, PA 19104 (USA)
E-mail: chrischen@seas.upenn.edu

© 2007 WILEY-VCH Verlag GmbH & Co. KGaA, Weinheim

WILEY InterScience®
DISCOVER SOMETHING GREAT

area are altered, which may affect how cells form adhesions and exert force through them.

Here, we set out to investigate cell spreading and traction forces with a range of post diameters, center-to-center spacings and stiffnesses. We designed nine different post array geometries with post diameters ranging from 0.75 to 1.5 μm, and center-to-center spacings ranging from 1.5 to 4.5 μm, collectively referred to as nanopost arrays (Fig. 1). To capture a wide range of post stiffnesses, we aimed for a post height of 3 μm. Based on Equation 1, these dimensions capture a range of post stiffnesses from 4.6 to 74 nN μm^{-1}, which encompasses post stiffness values previously reported in literature.[15,16,18,19] We used i-line projection photolithography to pattern these post array geometries on the same silicon wafer, followed by deep reactive ion etching (DRIE) of exposed silicon. To eliminate the problem of clogging silicon masters when casting with poly-

dimethylsiloxane (PDMS), we etched silicon posts rather than holes, and generated positive replicas of these nanopost arrays by double casting with PDMS (Fig. 1a). When these PDMS nanopost arrays were examined with scanning electron microscopy, we observed post sidewalls that tapered out at the base and were not completely vertical. Moreover, post height varied between the different array geometries, with the shortest posts found in the array geometries with target post diameters of 1.5, 1 and 0.75 μm and center-to-center spacings of 2.5, 2 and 1.5 μm, respectively (Fig. 1b–d). Array geometries with greater center-to-center spacings were found to have taller posts closer to the intended height of 3 μm (Fig. 2a–f). These results agree with published literature on the pattern density-dependence of DRIE, also known as microloading, in which low pattern density geometries etch faster than high pattern density geometries.[20]
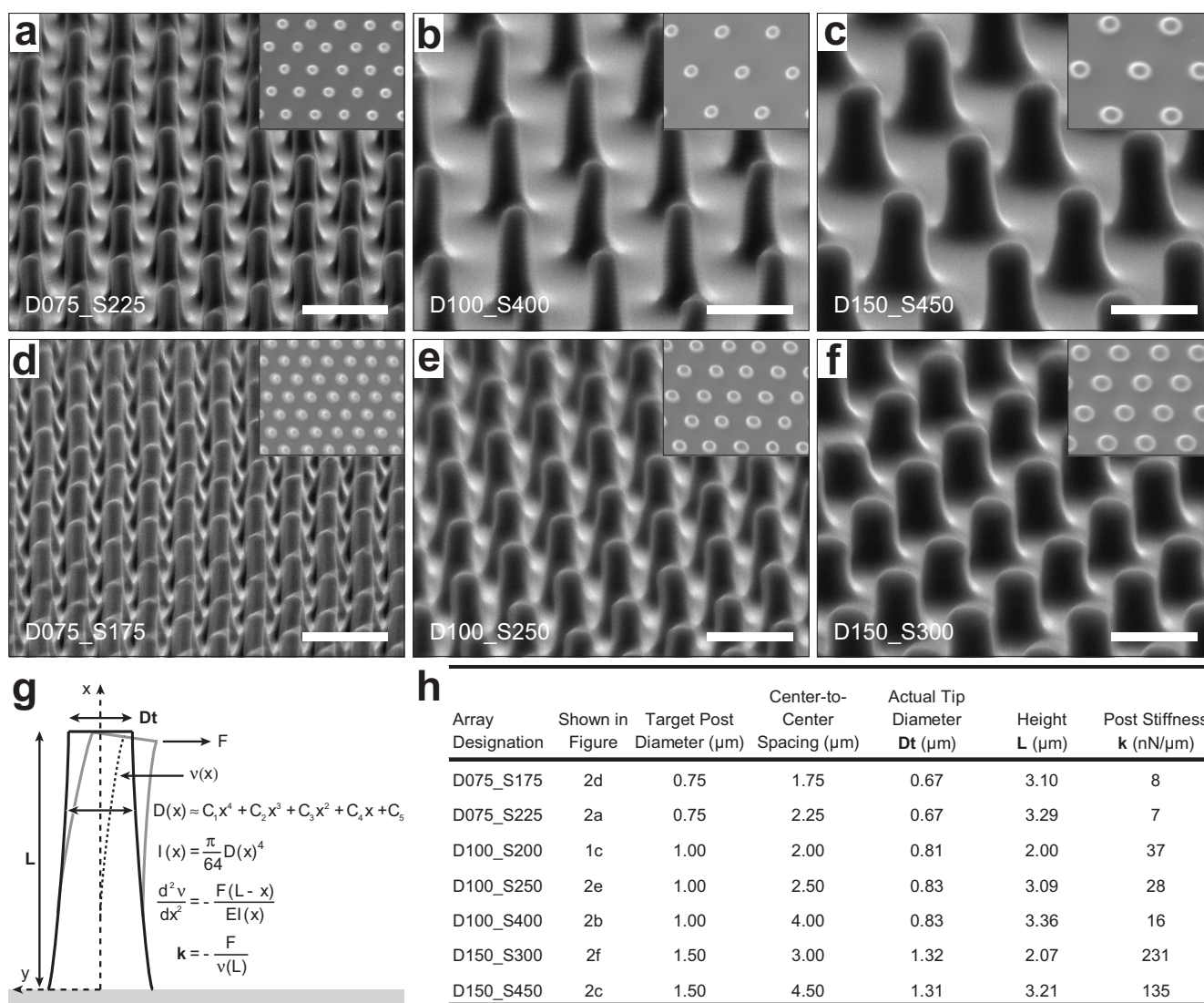

Array Designation	Shown in Figure	Target Post Diameter (μm)	Center-to-Center Spacing (μm)	Actual Tip Diameter D_t (μm)	Height L (μm)	Post Stiffness k (nN/μm)
D075_S175	2d	0.75	1.75	0.67	3.10	8
D075_S225	2a	0.75	2.25	0.67	3.29	7
D100_S200	1c	1.00	2.00	0.81	2.00	37
D100_S250	2e	1.00	2.50	0.83	3.09	28
D100_S400	2b	1.00	4.00	0.83	3.36	16
D150_S300	2f	1.50	3.00	1.32	2.07	231
D150_S450	2c	1.50	4.50	1.31	3.21	135

Figure 2. Characterization of elastomeric nanopost arrays. a–f) SEM images of PDMS nanopost arrays. Insets show top-down images of arrays. Scale bar is 3 μm. g) Calculation of post stiffness for a post with varying cross-sectional diameter. h) Table summarizing post measurements and calculated stiffness for different post array geometries.

We measured the post diameters and heights for seven out of nine post array geometries (Fig. 2h), with the other two post array geometries deemed unsuitable due to severe microloading effects. As a convention, we refer to each array geometry by a designation (e.g. D075_S225 is a post array with a post diameter of 0.75 μm and center-to-center spacing of 2.25 μm). In all array geometries, the actual diameter at the tip of the posts was less than the intended diameter, while base diameters were 0.5–1 μm larger than the tip diameter. The sidewall profiles of the posts, despite not being vertical, were also not linear near the base. Thus, the force-displacement relationship described in equation 1 for an ideal cylindrical beam could not be used to determine the post stiffnesses for these different post arrays. To calculate a more accurate value for the stiffness of the different posts, we fit a polynomial expression to describe diameter $D(x)$ as a function of the x axis which passes through the neutral axis of a post (Fig. 2g). $D(x)$ is substituted into $I(x)$, the second moment of area for a beam with a circular cross section, which subsequently is substituted into the moment-curvature equation, where curvature is d^2v/dx^2 and post deflection is $v(x)$. Using an arbitrary force F, the measured post height L, a Young's modulus E of 2.5 MPa, and boundary conditions of $v(0) = 0$ and $dv'(0) = 0$, the moment-curvature equation is double integrated numerically in MATLAB, to obtain a numerical expression for the post deflection due to a bending force. We equate the post stiffness k to F divided by the post deflection at the tip. With the seven characterized post array geometries we were able to achieve post stiffnesses ranging from 7 to 231 nN μm^{-1} (Fig. 2h).

To investigate whether cells cultured on these different post array geometries adhere, spread and contract differently, we cultured cells on the nanopost arrays for 14 hours and then fixed the cells and stained for F-actin. Cells cultured on the nanopost arrays looked similar to those on flat continuous surfaces, with ruffled lamellipodia (Fig. 3 a–c). Furthermore, we found the average spread area of cells on the different post array geometries to be the same as that of cells on flat surfaces (Fig. 3d). These data suggest that the post array geometries that we tested do not affect cell spreading any differently from a flat, continuous substrate.

To investigate whether cells generated different amounts of traction force on these post arrays, we collected fluorescence image stacks of the tip and base of the posts. We wrote image analysis software in MATLAB to detect post deflections from these images. For cells cultured on arrays D150_S300 and D150_S450, we were not able to detect post deflections above the background noise. Thus we concluded that these arrays, having post stiffnesses of 231 and 135 nN μm^{-1}, respectively, were too stiff for measuring traction forces. Tan et al previously used a post stiffness of 32 nN μm^{-1} and du Roure et al used post stiffnesses ranging from 1.3 to 21.8 nN μm^{-1}.[15,18] Consequently, we
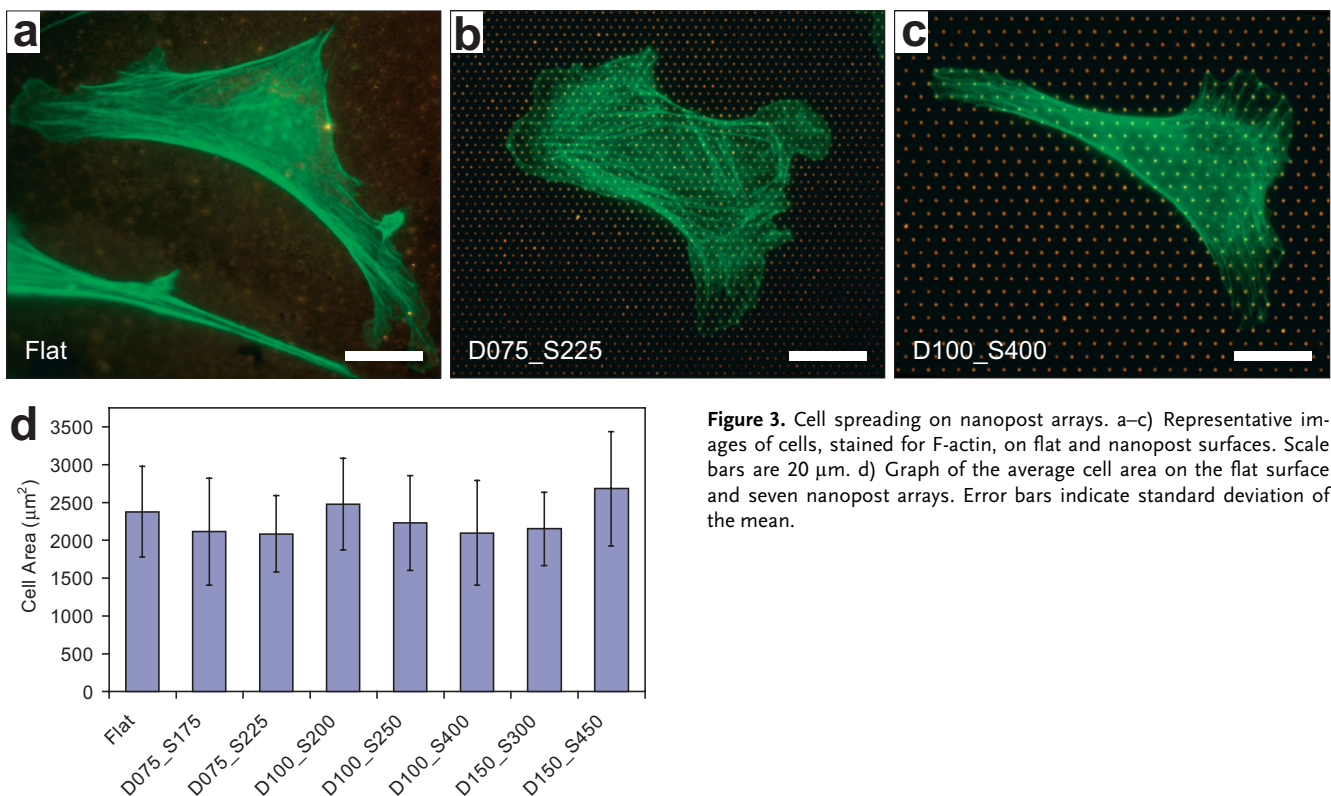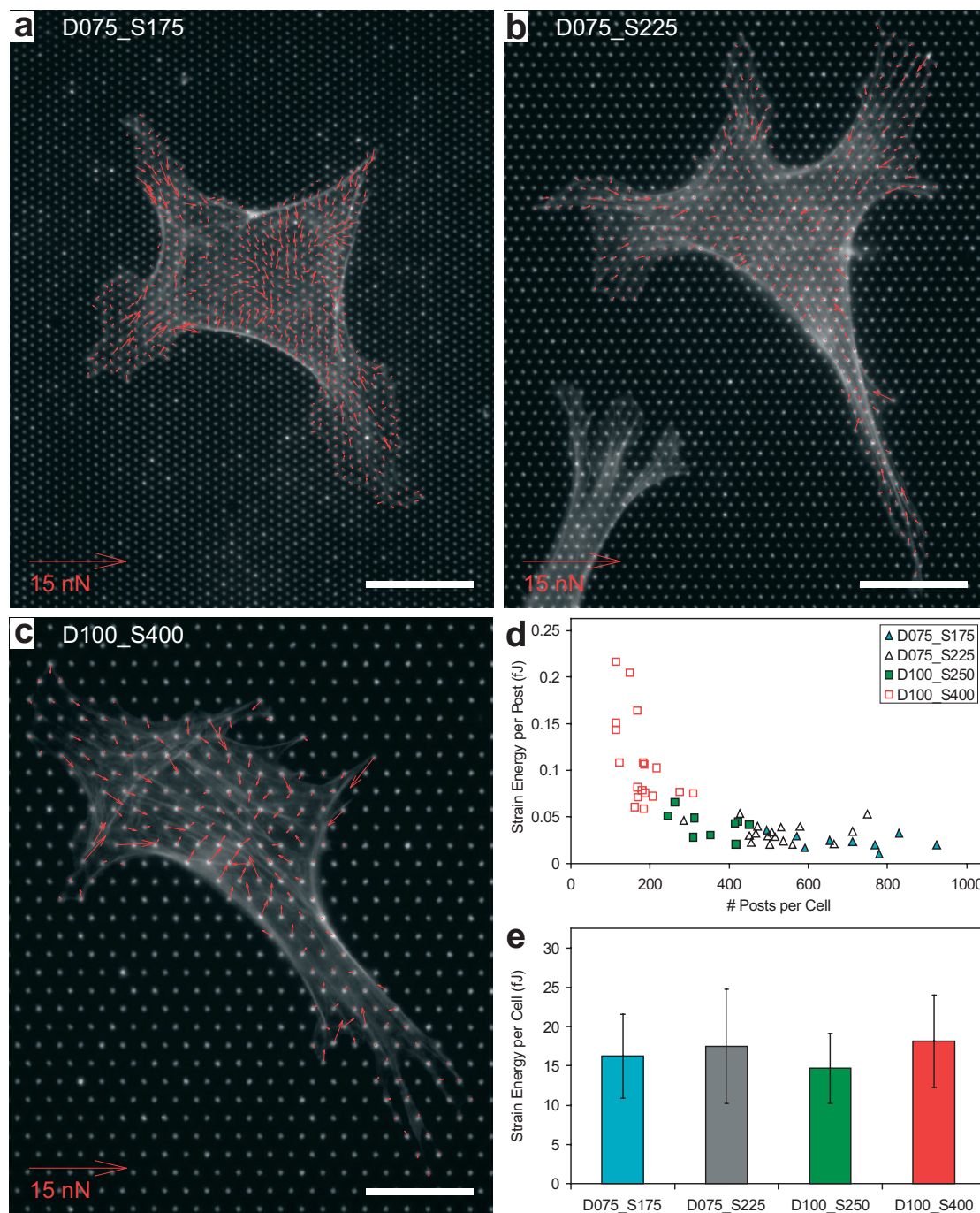

Figure 3. Cell spreading on nanopost arrays. a–c) Representative images of cells, stained for F-actin, on flat and nanopost surfaces. Scale bars are 20 μm. d) Graph of the average cell area on the flat surface and seven nanopost arrays. Error bars indicate standard deviation of the mean.

analyzed traction forces on arrays D075_S175, D075_S225, D100_S250, and D100_S400, which have post stiffnesses of 8, 7, 28 and 16 nN μm^{-1}, respectively. Representative force vector plots of single cells suggest that post density influences the magnitude of force on each post with the greatest forces per post found on D100_S400 (Fig. 4a–c). Interestingly, we also observed weaker traction forces under the lamellipodial regions compared to forces found several microns inside the edge of the

cells. To quantitatively measure cellular contractility, we calculated the strain energy for each post under a cell, $u(i)$:

$$u(i) = \frac{1}{2}k\delta(i)^2 \qquad (2)$$

where $\delta(i)$ is the displacement of the ith post. We found that the average of $u(i)$ for a cell has an inverse relationship with the number of posts underneath that cell (Fig. 4d). As a con-

Figure 4. Traction force measurement on nanopost arrays. a–c) Representative force vector plots overlayed on cells spread on different nanopost array geometries. White scale bars are 20 μm. d) Graph of the strain energy per post versus the number of posts per cell. e) Graph of the average strain energy per cell on four nanopost arrays. Error bars indicate standard deviation of the mean.

sequence, the strain energy per cell, which is found by summing $u(i)$, is statistically the same across the different post array geometries (Fig. 4e). We infer from this data that cellular work may be unaffected by post geometry presentation. These findings suggest that increasing the number of sensors per cell will increase spatial resolution, but will also require increased sensitivity to ever-smaller forces.

In conclusion, we developed nine different post arrays, some with the smallest post diameters reported thus far for use with traction force experiments. In contrast to other studies that used deep reactive ion etching to fabricate silicon post array masters, we opted to create posts instead of holes.[18,19] Because DRIE is increasingly affected by microloading and aspect-ratio-dependent effects when etching extremely high density patterns,[20] we obtained posts with sidewall profiles unlike any reported elsewhere. Despite these complicating results, we were able to calculate the stiffnesses of the posts. We investigated the area and morphology of cells cultured on these different nanopost arrays and concluded that cell spreading on these surfaces was similar to that found on continuous tissue culture substrates. Four out of nine nanopost arrays were suitable for traction force measurements and we observed that the strain energy per cell was constant across the different arrays. In the future, the nanopost arrays could be used to investigate other functional outputs of cells, such as forces exerted during migration and spreading of the lamellipodia. We believe the nanopost arrays represent a significant advance in post array-based tools for measuring traction forces.

Experimental

Fabrication and Characterization of Nanoposts: Silicon wafers were spin-coated with photoresist (SPR-220, Rohm and Haas) and then patterned via projection photolithography (AS200 5x i-line stepper, GCA). After photoresist development, exposed silicon was deep reactive ion etched (Centura 5200 etcher, Applied Materials) to form arrays of submicron-to-micron scale pillars with near-vertical sidewalls. Silicon wafers were rinsed in acetone to remove the remaining photoresist and then diced into silicon masters for subsequent replica-molding. Silicon masters were then cleaned in Piranha solution and silanized with tridecafluoro-1,1,2,2-tetrahydrooctyl)-1-trichlorosilane (United Chemical Technologies). To cast silicone nanopost arrays, replica-molding of the silicon masters was performed as previous described.[15] Briefly, liquid PDMS prepolymer (Sylgard 184, Dow-Corning) was poured over a silicon master, cured at 110 °C for 15 minutes, and peeled to create a negative replica containing an array of holes.[21] The negative replica was plasma-oxidized and silanized to facilitate subsequent release of PDMS from the replica. PDMS prepolymer was poured over the negative replica and cured at 110 °C for 20 h, after which the nanopost arrays were peeled from the negative replica. PDMS nanopost arrays were imaged in a scanning electron microscope (HRSEM, JEOL 6300F) to obtain geometric measurements for post stiffness calculations.

Cell Culture: NIH/3T3 mouse fibroblasts (ATCC CRL-1658) were cultured in Dulbecco's modified Eagle's medium containing 2 mM L-glutamine, 100 U ml^{-1} penicillin, and 100 mg ml^{-1} streptomycin with 10% bovine serum (Invitrogen).

Culture of Cells on Nanopost Arrays: Nanopost substrates were prepared for cell attachment as previously described.[15] Briefly, fibronectin (50 μg ml^{-1}; BD Biosciences) was adsorbed onto a PDMS stamp, dried, and then placed in contact with ozone-treated post arrays (ozone cleaner; Jelight), allowing fibronectin to transfer onto the tops of the posts.[22]

The arrays were fluorescently labelled with 5 μg ml^{-1} of Δ^9-DiI (Invitrogen) and blocked from protein adsorption with 0.2% Pluronics F127 NF (BASF). Cells were seeded onto arrays of posts, allowed to spread overnight for 14 h, fixed with 3.7% paraformaldehyde and stained with Alexa Fluor 488 phalloidin (Invitrogen) to visualize F-actin.

Quantification of Traction Forces: Cell areas were determined using image analysis software written in MATLAB (Mathworks). Briefly, fluorescent images of the F-actin cytoskeleton were collected for each cell using a 63x objective (NA 1.4) on an Axiovert 200M microscope (Carl Zeiss). An edge filter was then used to detect the presence of actin filaments in each image. Detected objects were binarized and interior pixels filled in to obtain the cell area.

Quantification of Cell Area: Traction forces were determined using image analysis software written in MATLAB. Briefly, fluorescent image stacks of the base and tip of posts were collected for each cell. Intensity profiles for images of posts at the base and tip were modelled as two-dimensional Gaussians, and the position of each post was determined by a non-linear least squares fit to this model. The undeflected positions of posts were determined by images of the focal plane at the base of posts. To account for global shifts in the image stack, the grid of centroids in the base focal plane is aligned with the grid of centroids in the tip focal plane, such that deviations are minimized between the base and tip positions of posts not attached to cells. Using this method, post displacements on the order of 30 nm can be detected. Displacement vectors were converted to force vectors using the post spring constant k (Fig. 2h), derived from SEM measurements.

[1] D. A. Lauffenburger, A. F. Horwitz, *Cell* **1996**, *84*, 359.

[2] C. S. Chen, M. Mrksich, S. Huang, G. M. Whitesides, D. E. Ingber, *Science* **1997**, *276*, 1425.

[3] A. J. Engler, S. Sen, H. L. Sweeney, D. E. Discher, *Cell* **2006**, *126*, 677.

[4] J. R. Couchman, D. A. Rees. *Cell Biol. Int. Rep.* **1979**, *3*, 431.

[5] S. Miyamoto, S. K. Akiyama, K. M. Yamada, *Science* **1995**, *267*, 883.

[6] D. Raucher, M. P. Sheetz, *J. Cell Biol.* **2000**, *148*, 127.

[7] G. Giannone, B. J. Dubin-Thaler, H. G. Dobereiner, N. Kieffer, A. R. Bresnick, M. P. Sheetz, *Cell* **2004**, *116*, 431.

[8] W. M. Chrzanowska, K. Burridge, *J. Cell Biol.* **1996**, *133*, 1403.

[9] N.Q. Balaban, U. S. Schwarz, D. Riveline, P. Goichberg, G. Tzur, I. Sabanay, D. Mahalu, S. Safran, A. Bershadsky, L. Addadi, B. Geiger, *Nat. Cell Biol.* **2001**, *3*, 466.

[10] A. Engler, L. Bacakova, C. Newman, A. Hategan, M. Griffin, D. Discher, *Biophys. J.* **2004**, *86*, 617.

[11] D. Lehnert, B. Wehrle-Haller, C. David, U. Weiland, C. Ballestrem, B. A. Imhof, M. Bastmeyer, *J. Cell Sci.* **2004**, *117*, 41.

[12] A. K. Harris, P. Wild, D. Stopak, *Science* **1980**, *208*, 177.

[13] R. J. Pelham, Jr., Y. Wang, *Mol. Biol. Cell* **1999**, *10*, 935.

[14] M. Dembo, Y. L. Wang, *Biophys. J.* **1999**, *76*, 2307.

[15] J. L. Tan, J. Tien, D. M. Pirone, D. S. Gray, K. Bhadriraju, C. S. Chen, *Proc. Natl. Acad. Sci. USA* **2003**, *100*, 1484.

[16] K. A. Addae-Mensah, N. J. Kassebaum, M. J. Bowers II, R. S. Reiserer, S. J. Rosenthal, P. E. Moore, J. P. Wikswo, *Sens. Actuators A* **2007**, *136*, 385..

[17] M. Madou, *Fundamentals of Microfabrication: The Science of Miniaturization*, Ed. 2, CRC Press, Boca Raton, FL **2002**.

[18] O. du Roure, A. Saez, A. Buguin, R. H. Austin, P. Chavrier, P. Silberzan, B. Ladoux, *Proc. Natl. Acad. Sci. USA* **2005**, *102*, 2390.

[19] Y. Zhao, X. Zhang, *Sens. Actuators A* **2006**, *125*, 398.

[20] R. Gottscho, A. Jurgensen, D. J. Vitkavage, *J. Vac. Sci. Technol. B* **1992**, *10*, 2133.

[21] Y. Xia, G. M. Whitesides *Angew. Chem. Int. Ed.* **1998**, *37*, 550.

[22] J. L. Tan, W. Liu, C. M. Nelson, S. Raghavan, C. S. Chen, *Tissue Eng.* **2004**, *10*, 865.